Available online at www.sciencedirect.com
ScienceDirect
Journal of the European Ceramic Society 30 (2010) 2397–2405
www.elsevier.com/locate/jeurceramsoc

Oxidation of ZrB_2–SiC–$ZrSi_2$ ceramics in oxygen

Oleg N. Grigoriev [a], Boris A. Galanov [a], Vladimir A. Lavrenko [a], Alla D. Panasyuk [a], Sergey M. Ivanov [a,*], Alexandr V. Koroteev [a], Klaus G. Nickel [b]

[a] *Institute for Problems in Materials Science of NAS of Ukraine, Kiev 04192, 3 Krzhyzhanovsky str., Ukraine*
[b] *Tuebingen University, Tuebingen 72074, 56 Wilhelmstraße, Germany*

Available online 1 May 2010

Abstract

The oxidation of ZrB_2–SiC and ZrB_2–SiC–$ZrSi_2$ ceramics of different composition has been studied experimentally at 1500 °C in pure oxygen for up to 50 h. ZrB_2–SiC–$ZrSi_2$ ceramics proved to be the most oxidation-resistant at $ZrSi_2$ contents of less then 4 wt%. These ceramics were more oxidation-resistant than ZrB_2–SiC ceramics. An analytical model of growth kinetics for a multilayered scale based on an oxidation–diffusion balance was developed and tested.

Keywords: D. Borides; B. Composites; D. SiC; D. Silicides; Oxidation

1. Introduction

The introduction of silicon carbide into ZrB_2 (20–25 vol.%) improves its resistance to high-temperature oxidation. The protective oxide film in the ZrB_2–SiC system consists of a continuous and dense corrosion-resistant (SiO_2–B_2O_3) glassy film with fine grains of ZrO_2 scattered in it. The research has shown that the ZrB_2–$ZrSi_2$ system is characterized by a lower oxidation rate compared with pure ZrB_2.[1,2] Addition of silicides of Zr, Mo, Ta, or others transition metals improve sinterability, as well as strength and oxidation resistance of ZrB_2–SiC ceramics.[3–8] The disilicide additives proved to be especially efficient because they are alternative (beside SiC) sources of silicon for SiO_2 formation. The enhanced oxidation resistance of ceramics with silicide additives may be explained in the following ways: (1) the metal oxide, for example Ta_2O_5, formed by oxidation of $TaSi_2$, in the borosilicate glass leads to formation of immiscible phase-separated glasses with higher viscosity and lower permeability to oxygen;[3,9] (2) metal addition (in particular, Ta) results in substitution of Ta onto Zr sites in ZrO_2, which reduces the concentration of oxygen vacancies and decreases the rate of oxygen transport through the growing scale;[8] and (3) in the presence of silicides ($ZrSi_2$, $MoSi_2$, $CrSi_2$), $ZrSiO_4$ forms during oxidation and promotes an increase in oxidation resistance.[1,2]

In this paper we consider oxidation processes for UHTCs in the ZrB_2–SiC($ZrSi_2$) system. It is known that $ZrSi_2$ additives (20–40 vol.%) promote sintering activation with formation of dense ceramics even at 1550 °C.[7,10] The range of application of such ceramics is limited due to the low melting temperature of $ZrSi_2$. In this study the amount of silicide additive is limited to 14 wt%, which is enough for liquid-phase sintering of these ceramics at $T > 1800$ °C. The main goal of the current research is the investigation of ability of a silicide additive ($ZrSi_2$) in ZrB_2–SiC ceramics to decrease the oxidation rate at temperatures above 1400 °C. In addition, a new oxidation model based on the available experimental data is presented.

2. Materials and methods

The α-SiC powder used in the study was UF10 grade produced by the H.C. Starck Company, Germany. The ZrB_2 and $ZrSi_2$ powders were synthesized at the Institute for Problems in Materials Science (IPMS) using carbothermal reduction of the appropriate oxides. The obtained powders were characterized by X-ray diffraction (XRD) and chemical analyses. Typical ZrB_2 powder contained 78.8 wt.% B and <0.1 wt.% O. Powder batches contained up to 0.7 wt% C which corresponded to 3.5 wt% B_4C. It is known that in the system under study the boron carbide additive promotes ceramics sintering.[11] $ZrSi_2$ powder had the following chemical composition: 61.0 wt% Zr, 37.0 wt% Si, <0.1 wt% Fe and 0.5 wt% residual solids that were insoluble in acids. Both powders had a particle size in the range 5–20 μm.

* Corresponding author.
E-mail addresses: ism@ipms.kiev.ua, ism@voliacable.com (S.M. Ivanov).

0955-2219/$ – see front matter © 2010 Elsevier Ltd. All rights reserved.
doi:10.1016/j.jeurceramsoc.2010.03.016

Sintering studies were performed in order to obtain ceramics with an average grain size of about 15–20 μm to minimize high-temperature creep. Grinding of powders was carried out using an acetone medium and ZrB_2 grinding balls. Grinding balls were made from pure powders by hot pressing. The lining of the mill was fabricated out of a caprolactone wear-resistant polymer. The powders were ground to a starting average particle size of ∼3 μm. Final milling and blending of charge components were done in a planetary ball mill. Optimum particles dispersions were obtained by planetary milling for 5–9 h, providing sufficiently small grain sizes for hot pressing (from 2.5 to 1.1 μm, respectively), as determined by a laser particle size analyzer (Laser Micron Sizer, Japan).

Hot pressing was conducted using an induction heating unit in graphite dies in the ambient atmosphere, although the powders inside the dies were presumed to be protected by the in situ generation of a protective CO/CO_2 gas mixture within the die. The temperature of isothermal sintering under load was in the range of 1800–2150 °C, pressure—26–30 MPa, time of isothermal densification 15–40 min, heating rates—up to 100 °C/min. By the end of isothermal holding the axial pressure was released, ceramics were cooled in the die at the rate of 35 °C/min down to 1200–1500 °C. Next, ceramics together with the die were placed in a graphite container to cool down to room temperature.

In contrast to vacuum hot pressing, sintering of ceramics without a protective chamber takes place under conditions of partially reducing media $CO–CO_2$, resulting from oxidation of the graphite dies. During hot pressing, a number of chemical reactions occur between the residual oxide phases of the charge (SiO_2, ZrO_2, B_2O_3), boron carbide (reducing oxides), as well as CO. The experimental data show that removal of oxide impurities occurred during sintering, accompanied by generation of a secondary ZrB_2 phase and a decrease in B_4C content along with a considerable evolution of volatile oxidation products (SiO, B_2O_3, CO_2, etc.). The evolution was achieved by holding the sample isothermally at intermediate temperatures, and by applying the maximum pressures at the final stage of the process.

In order to study the impact of $ZrSi_2$ on the structure and properties of ZrB_2–SiC ceramics, it was introduced in amounts up to 14 vol.%, which is greater than commonly required for sintering additives (3–5 vol.%). Compositions with 51 vol.% ($ZrB_2 + ZrSi_2$) + 49 vol.% SiC ceramics were chosen for the present study of oxidation behaviour. The ZrB_2:$ZrSi_2$ ratios and the sample designations are summarized in Table 1.

The microstructure and phase composition of ceramics and oxide scales were studied using the XRD method (HZG-4 (Germany) and DRON-4 (Russia) diffractometers with filtered radiation of Fe and Cu anodes in point-by-point scanning mode), light-optical and scanning electron microscopy (Superprobe 733, JEOL, Japan). The "New_Profile" XRD analysis program package[12] as well as PDF-2 database were used for qualitative and quantitative phase composition analysis. The chemical composition of the phases formed was inferred from energy dispersive X-ray spectroscopy (EDX, Link, England).

Oxidation experiments for ZrB_2–SiC and ZrB_2–SiC-$ZrSi_2$ ceramics were carried out in Tuebingen University, Germany. Oxidation was studied in pure oxygen at a temperature of 1500 °C. A computer controlled furnace (Bahr) was used for the following heating-atmosphere cycle:

1. Heating at 10 K/min in argon up to 1400 °C;
2. heating at 2 K/min in argon up to 1500 °C;
3. exposure of samples at 1500 °C in oxygen with a flow rate of 0.1 l/min in 40 mm tube;
4. cooling at 2 K/min in argon up to 1400 °C;
5. cooling at 10 K/min in argon to room temperature.

Samples were held at 1500 °C in flowing oxygen for 0.5, 3, 15, 30 and 50 h. Before the thermal treatment and after every thermal cycle all the samples were weighed (Sartorius ultra-balance). Thus, the change of sample mass gain was measured gravimetrically during high-temperature oxidation. Samples were 10 mm by 5 mm by 2 mm.

3. Results and discussion

3.1. Structure of ceramics

In order to study the interaction of zirconium boride with zirconium silicide, ZrB_2 mixed with 20 vol.% silicide was hot pressed in the temperature range of 1600–2100 °C. X-ray diffraction analysis (not shown) revealed that small amounts of SiC (3C) and a new phase with a cubic lattice were formed. Lattice parameters of the new phase were intermediate between the parameters of ZrC and ZrO cubic phases. In the XRD patterns for the hot-pressed ZrB_2–$ZrSi_2$–SiC system with different component ratios, beside the ZrB_2 and SiC phases, the same cubic phase with variable lattice parameters was present (Fig. 1a). The ZrB_2 lattice parameters were unchanged and, therefore, solid solutions based on ZrB_2 were not formed.

The equilibrium phase diagram for the Zr–Si system[13] points out to a peritectic type of $ZrSi_2$ decomposition with the appearance of a Zr–Si liquid phase at hot pressing temperatures exceeding 1620 °C. The interaction of the Zr–Si liquid with the basic phases of the composite, besides the interaction with CO, leads to the formation of a new phase with the ZrC lattice structure, and some other intermediate compounds as well as

Table 1
The ZrB_2:$ZrSi_2$ ratio for ceramic composites.

	Marking index							
	US-4	USS-4	USS-41	USS-42	USS-43	USS-44	USS-45	USS-46
ZrB_2 vol.%	100	92	96	93	86	81	76	73
$ZrSi_2$ vol.%	0	8	4	7	14	19	24	27

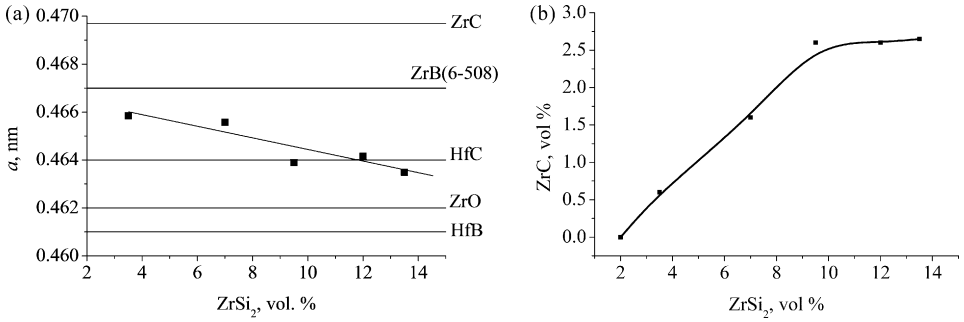

Fig. 1. (a) Lattice parameters of the cubic phase in comparison with known ones. (b) Dependence of cubic phase volume content from $ZrSi_2$ volume content in the charge.

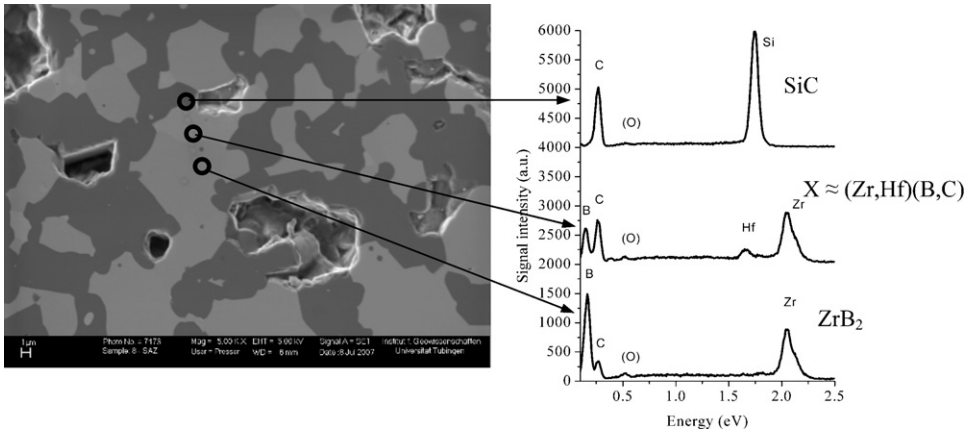

Fig. 2. EDX spectrum of 3rd phase grain, as well as spectra of SiC and ZrB_2 grains.

enrichment of the liquid with boron. The smaller lattice parameter of the new phase (Fig. 1a), compared with zirconium carbide, and direct observations of Zr, C, and B presence in grains (with different contrast relatively ZrB_2 grains) by EDX-method (Fig. 2) are caused by formation of solid solutions in Zr(C,B) system. The XRD data shows that the volume content of the new cubic phase does not exceed 3% (Fig. 1b), which qualitatively corresponds to microscopic observations. The linear dependence between $ZrSi_2$ and Zr(C,B) contents exists only up to ~10 vol.% $ZrSi_2$ (Fig. 1). XRD shows that in ceramics with high $ZrSi_2$ content (>10 vol.%) residual Zr–Si liquid is partially crystallized during cooling as zirconium silicide $ZrSi_2$ with higher lattice parameters (compared to the initial state), and partially remains in amorphous state. Thus, for small silicide additions, the liquid phase is almost entirely consumed by the Zr(Hf)C(B) phase. However, higher zirconium silicide contents lead to an excess of Zr–Si–B–(O) liquid, which on cooling transforms into residual amorphous phase and modified crystalline zirconium silicide.

The microstructure of fabricated samples is presented in Fig. 3. The porosity of US4 samples was about 4–5%, porosity less than 1% for lower $ZrSi_2$ content (2–4 vol.% USS4–USS42), and with porosity increase up to 6% at higher $ZrSi_2$ content

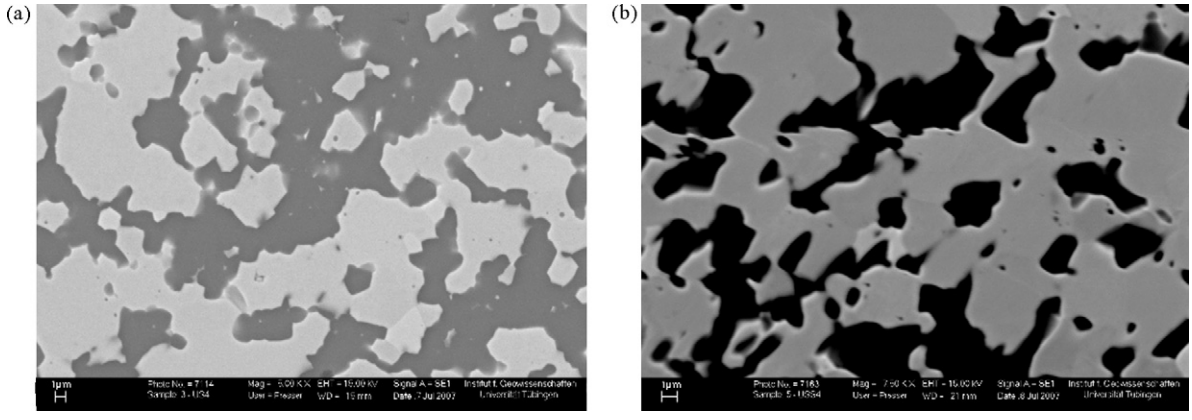

Fig. 3. Microstructure of the ceramics of different compositions: US4 (a); USS4 (b).

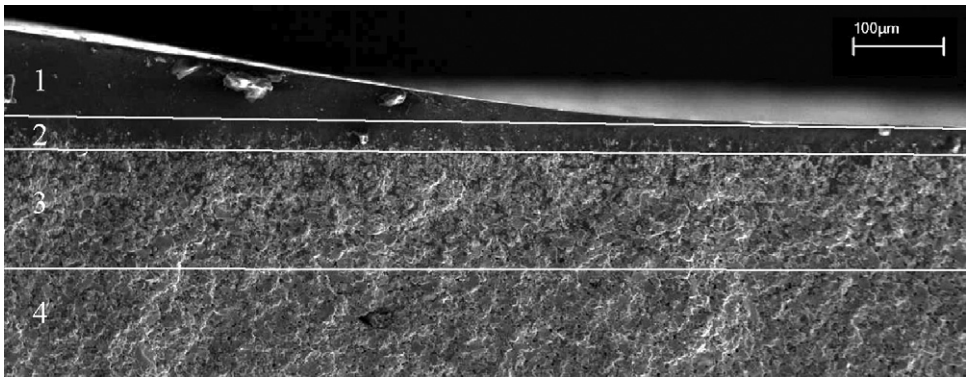

Fig. 4. Cross section SEM images of oxide scale layers: layer 1 (the outer layer)—$SiO_2 + B_2O_3$; layer 2—dense zirconia–silica; layer 3—silicon carbide depleted, zirconia (zircon) zone with a graded increase in ZrB_2 content through its thickness; and layer 4—unaltered ZrB_2–SiC.

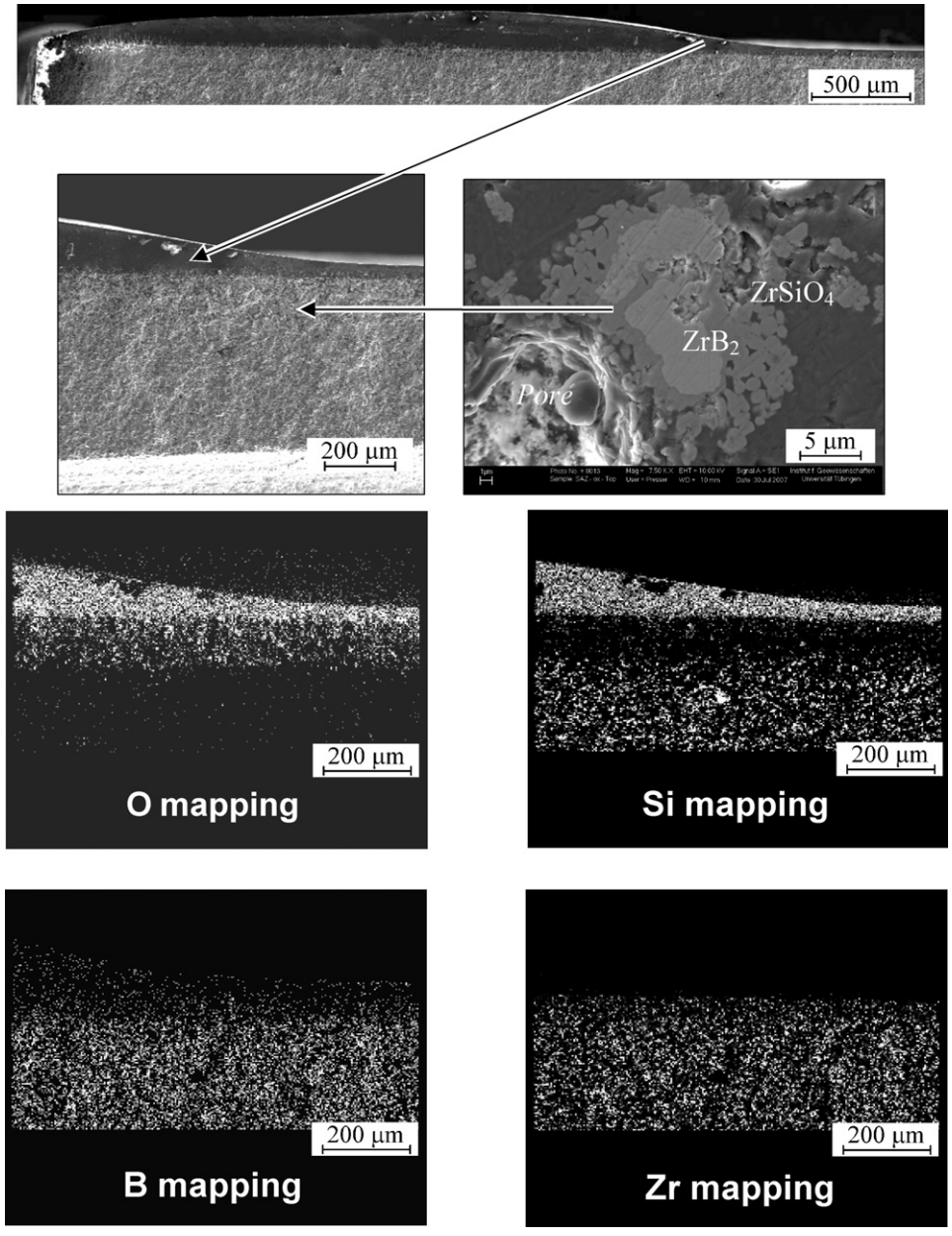

Fig. 5. Cross sectional images and elemental mapping of a typical oxidation scale.

(USS44–USS46). In all cases grain sizes of the main phases (silicon carbide, zirconium boride and Zr(Hf)C(B) phase) were in the range of 2–20 μm. The morphology of the ZrB_2 grains (deeply etched boundaries) after hot pressing indicates to the interaction of grains with the liquid phase (Fig. 3) since the consolidation itself is a reactive liquid-phase hot pressing process.

3.2. Experimental studies

An XRD study of ZrB_2–SiC and ZrB_2–SiC–$ZrSi_2$ ceramics after their oxidation did not show any qualitative differences among phase compositions (not shown). For both systems the oxidized surface layer contained an amorphous phase (borosilicate glass as indicated by the amorphous hump in the XRD pattern) as well as crystalline silica (cristobalite), zirconium oxide (baddeleyte), and $ZrSiO_4$ (zircon). Therefore, the differences in the oxidation kinetics of various ceramic systems must be analyzed to understand the quantitative differences of phase composition and structure of scale layers.

The typical structure of oxidized ZrB_2–SiC–$ZrSi_2$ is presented in Figs. 4 and 5. Elemental mapping of O, Si, Zr and B is shown in Fig. 5. Fig. 4 shows a typical three-layer scale formed on the surface after oxidation in oxygen for 50 h: layer 1 is borosilicate glass; layer 2 is dense zirconia–silica; layer 3 is silicon carbide depleted zirconia that has increasing ZrB_2 content through its thickness; and layer 4 is the unaltered ZrB_2–SiC matrix. Outer layer is non-homogeneous in thickness with discontinuities where bubble formation took place due to intensive gas emission. On the whole, the structure of surface oxidized layers corresponds to the structure described by Chamberlain et al.[14]

Mass gain was studied gravimetrically for ZrB_2–SiC and ZrB_2–SiC–$ZrSi_2$ (Fig. 6). The mass gains are characterized by nearly parabolic rate law dependence (especially for the 2nd system) which indicates diffusion control due to the dense oxide film formation. It is also obvious that the addition of $ZrSi_2$ to the ZrB_2–SiC ceramics leads to a significant decrease in mass gain (Fig. 6). For example, after 50 h at 1500 °C the mass gain decreased from ~27 mg/cm^2 for ZrB_2–SiC to ~9 mg/cm^2 for ZrB_2–SiC containing 4 vol.% $ZrSi_2$.

The oxidation resistance as a function of $ZrSi_2$ content in pure oxygen at 1500 °C was described by a curve with a minimum (Fig. 7). The increase of oxidation resistance at small

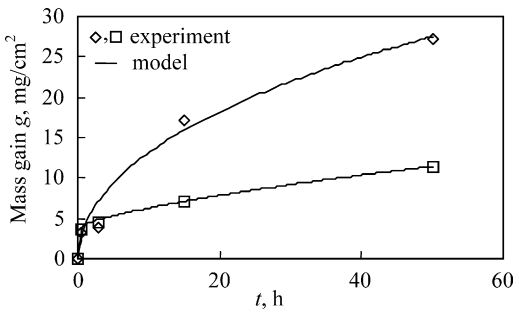

Fig. 6. Mass gain as a function of time in pure oxygen at 1500 °C for 51 vol.% ZrB_2–SiC (diamonds) and 46 vol.% ZrB_2–4 vol.% $ZrSi_2$–50 vol.% SiC (squares).

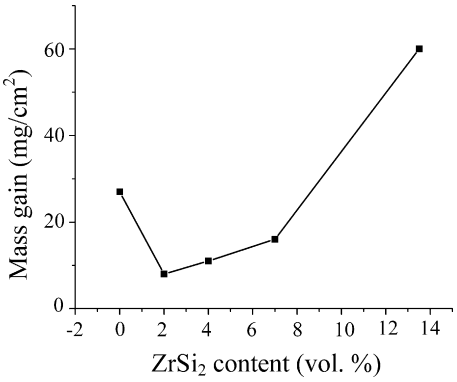

Fig. 7. The dependence of mass gain on $ZrSi_2$ content (vol.%) in charge for oxidation at 1500 °C for 50 h in oxygen.

additions of $ZrSi_2$ (up to 2 vol.%) requires additional analysis. The US4 and USS41 samples have approximately the same grain size of components but slightly different porosity contents (~5% and <1%, respectively). Therefore, the differences in oxidation rate could possibly be connected with differences of porosity and, in the final analysis, with the sintering activation effect on the account of the zirconium silicide additions. In addition, the Zr(Hf)C(B) phase is present in ZrB_2–SiC–$ZrSi_2$ ceramics (~3 vol.%) as solitary inclusions and does not form a continuous network. So, its presence alone should not influence the oxidation rate significantly. It may be supposed that the reduction of oxidation rate of the triple system with small content of $ZrSi_2$ may be also (along with porosity effect) connected with the inclusions and grain-boundary layers of residual amorphous Zr–Si–B phase that might form during $ZrSi_2$ decomposition under the scale of borosilicate glass. The interaction of oxygen with small amounts of amorphous phases may lead to the formation of additional protective SiO_2 and zircon phases. All these lead to the increase of ceramics oxidation resistance.

With the increase of $ZrSi_2$ content to more than 8 vol.% larger amounts of an unstable amorphous phase are present along with porosity along the grain-boundaries. These factors are likely responsible for a sharp rise in oxidation rate at higher $ZrSi_2$ contents.

3.3. Modeling

3.3.1. Model equations

The thickness and structure of the surface layers formed in oxygen at 1500 °C showed that the oxidation was almost parabolic. The oxide scale structure in ZrB_2–SiC and ZrB_2–SiC–$ZrSi_2$ systems corresponded to Chamberlain's model.[13] A schematic representation of the scale is shown in Fig. 8.

The main objective of the model is to simulate growth kinetics under isothermal conditions using multilayered flat scale structure with a given order and structure of layers. The scale is considered to be a multilayered continuum medium. Model hypotheses are the same as in detailed analysis of such systems by Dybkov.[15]

The basic model hypotheses are:

(1) the kinetics of scale growth are defined by chemical reactions at the layer boundaries and diffusion of species to the layer boundaries where chemical reactions take place and layer growth occurs;
(2) the changes of concentration c of diffusing substances in the layers occur with the negligibly low local speed ($\partial c/\partial t \approx 0$);
(3) chemical reactions at the layer boundaries occur with constant velocity;
(4) layers are macro-homogeneous, and because of this diffusion coefficients are constant (possibly, effective values in the case of micro non-homogeneity) and distributions of concentration of substances diffusing through individual layers are linear;

Oxidation is accompanied by a number of physical phenomena (including evaporation), which affect physical and chemical constants of the model (K_i, h_i).[15] Investigation of such effects is a separate task, which is beyond the scope of this work. It should be noted that the model implicitly takes into account such effects since the model constants are determined from experimental data.

If each layer of the scale is growing because of O_2 chemical transformations at the boundary with the next layer (more remote from the scale surface) and reduced because of similar transformations at the boundary with the previous layer (more close to the scale surface), then the Cauchy problem, which describes growth kinetics of the scale and takes into account the uncertainties of initial oxidation period, has the form:

$$\begin{cases} \dfrac{dL_1}{dt} = \left(\dfrac{1}{h_1} + \dfrac{L_1}{K_1}\right)^{-1} - \gamma_1\alpha\exp(-\beta t), \\ \dfrac{dL_2}{dt} = \left(\dfrac{1}{h_2} + \dfrac{L_2}{K_2}\right)^{-1} - \dfrac{dL_1}{dt} - \gamma_2\alpha\exp(-\beta t), \\ \dfrac{dL_3}{dt} = \left(\dfrac{1}{h_3} + \dfrac{L_3}{K_3}\right)^{-1} - \dfrac{dL_1}{dt} - \dfrac{dL_2}{dt} - \gamma_3\alpha\exp(-\beta t) \end{cases} \quad \begin{array}{l} L_1(0) = L_2(0) = L_3(0) = 0; \\ t \geq 0 \end{array} \tag{1}$$

(5) modeling of the kinetics of layer thicknesses changes is carried out on the basis of Evans time additivity principle[15,16]: the time dt required for a gain of layer thickness dL is the sum of time dt_c spent for chemical transformations on the layer boundary and time of oxygen diffusion dt_d to the place of chemical reactions: $dt = dt_c + dt_d$, where $dt_c = dL/h$, $dt_d = cdL/(-D\text{grad } c)$, h—layer growth rate stipulated by chemical reaction on the layer boundary L (chemical constant); c—O_2 concentration at the layer boundary; grad c—the gradient of O_2 concentration at the layer boundary; D–diffusion coefficient of oxygen.

As it follows from these hypotheses, O_2 concentrations and their values at the layer boundaries are unchanged during scale growth i.e. these values are constant.

The main constants entering into the system of model equations are chemical (h_i) and physical (diffusion, K_i) for each ith layer[15,16]: $K_i = D_i(c_{i(i+1)} - c_{i(i+1)})/c_{i(i+1)}$ where D_i—diffusion coefficient of oxygen in ith layer, c_{ij}—O_2 concentration in ith layer at the boundary with jth layer (see Fig. 8).

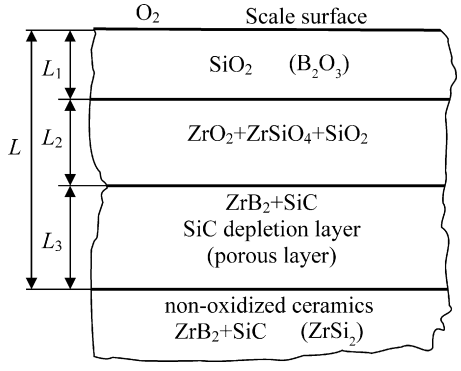

Fig. 8. Schematic of the oxide scale structure on the surface of ZrB_2-based ceramic safter oxidation in pure oxygen at 1500 °C.

where t—time; L_i (i = 1,2,3) is the layer thickness; $K_i > 0$, $h_i > 0$ are physical and chemical constants, respectively; $\gamma_i \leq 1$, i = 1, 2, 3—weight factors; constants $\alpha \geq 0$ and $\beta \geq 0$ take into account the uncertainty of the initial stage of oxidation. The parameter α can be considered as the random peak amplitude of deviation from average speed of scale growth and parameter β as the parameter determining the effective duration of initial stage of oxidation. Values of α and β, probably, depend on $ZrSi_2$ addition and evaporation as well.

The Cauchy problem (1) describes the growth kinetics of a scale with a given structure (which is defined by experiment or other methods based on the analysis of chemical reactions and their order in time), and not the formation of the structure itself.

Since scale growth begins from the 3rd layer then for a simplification we further assume $\gamma_1 = \gamma_2 = 0$, $\gamma_3 = 1$.

For given $h_i > 0$, $K_i > 0$, α, β the solution of system (1) defines layers thickness $L_i(t)$ at the current moment of time t i.e. their kinetics.

Thus, the main problem is to determine key parameters from the experimental kinetic curves: chemical and physical constants $h_i > 0, K_i > 0$ as well as parameters α and β that are coefficients in the differential equations of the Cauchy problems (1) and define growth kinetics of oxide scale.

3.3.2. Asymptotic analysis of model equations

Analysis as $t \to 0$. If the condition $h_3 - \alpha > 0$ is assumed then from (1) it follows that its solution at $t \to 0$ has the following asymptotics

$$\begin{aligned} &L_1(t) \approx h_1 t, \quad L_2(t) \approx (h_2 - h_1)t, \quad L_3(t) \approx (h_3 - h_2 - \alpha)t, \\ &L(t) = L_1(t) + L_2(t) + L_3(t) \approx (h_3 - \alpha)t. \end{aligned} \tag{2}$$

It can be seen from the latter relation (2) that the condition $h_3 - \alpha > 0$ defines an initial nonzero velocity of scale thickness

$L(t)$ growth. In addition, conditions

$$h_1 > 0, \quad h_2 - h_1 > 0, \quad h_3 - h_2 - \alpha > 0, \tag{3}$$

are conditions of formation of a three-layer scale at $t = 0$, and the left-hand parts of these inequalities define the initial velocity of the formation of each layer. The 3rd condition depends on a random factor α and can be true only when h_3–$h_2 > 0$. From this and from (3) the inequalities that can be deduced are: $h_3 > h_2 > h_1 > 0$, which have clear physical meaning and dictate the three-layer structure of the scale. During the initial stage of growth, chemical reactions dominate growth and their velocities are h_i, $i = 1, 2, 3$; the growth velocity of the 3rd layer h_3 should be higher than the growth velocity of the 2nd layer h_2, which, in turn, should be higher than the growth velocity of the 1st layer h_1. This is because the 1st layer is formed from the 2nd layer, the 2nd layer is formed from the 3rd, and the 3rd layer is formed from initial material. The parameter α can be seen as random amplitude of variation of the velocity of layer growth and, if inequalities (3) are true, then at sufficiently small values of α (i.e. at small random effects and lesser uncertainty) condition (3) will be satisfied.

Analysis at $t \to \infty$. As a result of investigation of system (1) the following estimates for scale layers thicknesses are obtained

$$\underline{L}_i(t) \le L_i(t) \le \bar{L}_i(t), \quad t \ge 0, \tag{4}$$

where functions $\underline{L}_i(t)$, $\bar{L}_i(t)$, $i = 1, 2, 3$ are determined by the equalities

$$\bar{L}_i(t) = -\frac{K_i}{h_i} + \sqrt{\left(\frac{K_i}{h_i}\right)^2 + 2K_i t}, \quad t \ge 0, \quad \underline{L}_1(t) = \bar{L}_1(t) + \frac{\alpha}{\beta}(\exp(-\beta t) - 1), \tag{5}$$

$$\underline{L}_2(t) = \bar{L}_2(t) - \bar{L}_1(t), \quad \underline{L}_3(t) = \bar{L}_3(t) - \bar{L}_2(t)$$

From (4) and (5) we have the following relations useful for kinetics analysis

$$\bar{L}_1(t) - \underline{L}_1(t) = \frac{\alpha}{\beta}(1 - \exp(-\beta t)) \ge 0,$$
$$\bar{L}_2(t) - \underline{L}_2(t) = \bar{L}_1(t) \ge 0,$$
$$\bar{L}_3(t) - \underline{L}_3(t) = \bar{L}_2(t) \ge 0, \quad t \ge 0,$$

and asymptotic at $t \to \infty$ equalities

$$\lim_{t\to\infty} \frac{\underline{L}_1(t)}{\bar{L}_1(t)} = 1, \quad \lim_{t\to\infty} \frac{\underline{L}_2(t)}{\bar{L}_2(t)} = 1 - \sqrt{\frac{K_1}{K_2}}, \quad \lim_{t\to\infty} \frac{\underline{L}_3(t)}{\bar{L}_3(t)} = 1 - \sqrt{\frac{K_2}{K_3}}. \tag{6}$$

Since from the physical point of view only positive boundaries should be considered in equalities (6) then from (6), the following inequalities can be deduced

$$K_1 \le K_2 \le K_3. \tag{7}$$

For the thickness of the whole scale $L(t)$ at $t \ge 0$ from equalities (5) we have estimates

$$\underline{L}(t) \le L(t) \le \bar{L}(t), \tag{8}$$

where

$$\bar{L}(t) = \sum_{i=1}^{3} \bar{L}_i(t), \quad \underline{L}(t) = \bar{L}_3(t) + \frac{\alpha}{\beta}(\exp(-\beta t) - 1),$$
$$\text{and } \lim_{t\to\infty} \frac{\bar{L}(t)}{\underline{L}(t)} = 1 + \sqrt{\frac{K_1}{K_3}} + \sqrt{\frac{K_2}{K_3}}.$$

The analysis shows that at $t \to \infty$ the dominant process in layer formation is oxygen diffusion (in relations (5) and (6) leading role are playing physical constants K_i, $i = 1, 2, 3$). From the model calculations follows that the outer layers (in our approximation SiO_2 and $ZrO_2 + ZrSiO_4 + SiO_2$) are rate-limiting step since diffusion constant K_1 in these layers is significantly lower than K_2 for layer $ZrB_2 + SiC$ (SiC depletion layer), see also (7) and Table 2.

From (4) and (5) at sufficiently large t the following inequalities are obtained

$L_i(t) \le \sqrt{2K_i t}$, $L(t) \le \sqrt{2Kt}$, where $L = L_1 + L_2 + L_3$, $K = (\sqrt{K_1} + \sqrt{K_2} + \sqrt{K_3})^2$. These inequalities mean that the growth of separate layers and the whole scale cannot be above parabolic growth, i.e. kinetic growth curves of layers and scales are below certain conventional parabolic kinetic curves which are determined by the constants h_i, K_i, K.

Thus, relations (2)–(8) can be used for determination of physical and chemical constants K_i, h_i, $i = 1, 2, 3$, as well as parameters α and β from experimental kinetic curves of growth of oxide scale layers. The use of these relations facilitates their search by numerical methods.

3.3.3. Numerical determination of parameters governing growth kinetics

If formation of a scale goes without volume changes or these changes can be neglected, then Eq. (1) may be re-written in terms

Table 2
Calculated model parameters.

Ceramics	K_1, mg^2/cm^4 h	h_1, mg/cm^2 h	K_2, mg^2/cm^4 h	h_2, mg/cm^2 h	α, mg/cm^2 h	β, 1/h
ZrB_2–SiC	0.82	0.26	47.2	289.5	10.9	0.0036
ZrB_2–SiC–$ZrSi_2$	1.75	0.93	8.16	125.9	0.29	0.0011

of mass gain (g):

$$\begin{cases} \dfrac{dg_1}{dt} = \left(\dfrac{1}{h_1} + \dfrac{g_1}{K_1}\right)^{-1}, \\ \dfrac{dg_2}{dt} = \left(\dfrac{1}{h_2} + \dfrac{g_2}{K_2}\right)^{-1} - \dfrac{dg_1}{dt}, \\ \dfrac{dg_3}{dt} = \left(\dfrac{1}{h_2} + \dfrac{g_3}{K_3}\right)^{-1} - \dfrac{dg_1}{dt} - \dfrac{dg_2}{dt} - \alpha\exp(-\beta t) \end{cases} \quad t \geq 0, \quad g_1(0) = g_2(0) = g_3(0) = 0\,, \tag{9}$$

where the constants $\alpha, \beta, h_i, K_i, i = 1, 2, 3$ differ from corresponding constants of (1) and have other dimensions; $g_i, \quad i = 1, 2, 3$ is mass gain per unit of surface area of ith layer, and $g = g_1 + g_2 + g_3$ is the mass gain of the whole sample per unit surface area.

Here we determine parameters $K_i, h_i, \quad i = 1, 2, 3, \alpha, \beta$ (see (9)) from experimental kinetic curves of oxide scale growth. However, in reality we have a limited set of experimental data which is presented in Fig. 6 and these are separate points belonging to kinetics curves $g(t)$ of the total scale growth, not to growth curves of individual layers. The structure of scale was characterized at discrete time intervals. Therefore, a simple problem is considered in which the 1st two layers are considered as, effectively, a single layer with combined characteristics K_1, h_1. This allows Eq. (9) to be reduced to the following Cauchy problem

$$\begin{cases} \dfrac{dg_1}{dt} = \left(\dfrac{1}{h_1} + \dfrac{g_1}{K_1}\right)^{-1} \\ \dfrac{dg_2}{dt} = \left(\dfrac{1}{h_2} + \dfrac{g_2}{K_2}\right)^{-1} - \dfrac{dg_1}{dt} - \alpha\exp(-\beta t) \end{cases}, \quad g_1(0) = g_2(0) = 0 \tag{10}$$

Recall that in (10) function g_1, K_1 and h_1 correspond to the effective external layer and g_2, K_2 and h_2 then become the properties of the 3rd layer (see Fig. 8).

Based on this combination, the function $g_1 = -(K_1/h_1) + \sqrt{(K_1/h_1)^2 + 2K_1 t}$ is a solution of the first Eq. (10) for the external effective layer, which has a parabolic growth kinetics. From this for definition of mass gain of internal layer $g_2(t)$ we have the Cauchy problem

$$\frac{dg_2}{dt} = \left(\frac{1}{h_2} + \frac{g_2}{K_2}\right)^{-1} - K_1\left(\left(\frac{K_1}{h_1}\right)^2 + 2K_1 t\right)^{-1/2} - \alpha\exp(-\beta t), \quad g_2(0) = 0 \tag{11}$$

The asymptotic analysis of solutions for Eqs. (10) and (11) can be done similar to one in the Section 3.3.2.

Eq. (11) most likely is not integrated in quadratures. Its approximated solution can be obtained by numerical methods. Its solution indicates that the growth of the layer is not parabolic.

A number of calculations using this model have been done to determine model parameters and validate functional dependencies. Data fitting was carried out with the least squares method where the objective function was the sum of squares of deviations of calculated mass gains from experimental ones. Initial data for the calculation of parameters of kinetic curves were taken from the experimental measurements of isothermal oxidation for 50 h at 1500 °C:

Diffusion and reaction constants (K_1, h_1, K_2, h_2) and constants taking into account uncertainties of initial oxidation period α and β, were calculated for ZrB_2–SiC and ZrB_2–SiC–$ZrSi_2$ and are presented in Table 2. Calculated kinetic curves are shown in Fig. 6 ($g = g_1 + g_2$). The addition of $ZrSi_2$ leads to the reduction of chemical reaction rate (h_2) by 2.3 and effective diffusion constant (K_2) by 5.8 times, the latter points to sharp decrease of oxygen diffusion in layer 2. These results correspond to the analysis of Figs. 6 and 7 in Section 3.2.

4. Conclusion

The investigations indicated that ZrB_2–SiC–$ZrSi_2$ ceramics with the optimal composition (2 wt% of $ZrSi_2$), had the best oxidation resistance for long-duration (50 h) exposure to pure oxygen at 1500 °C. The ZrB_2–SiC–$ZrSi_2$ ceramic had 3.4 times higher resistance to oxidation compared to the ZrB_2–SiC based on mass gain. In comparison with other non-oxide ceramics, such oxidation resistance is exceptionally high (the mass gain is <10 mg/cm^2 at 1500 °C after 50 h oxidation in pure oxygen). The oxidation process had kinetics that showed nearly ideal parabolic behaviour for long times.

The model of growth kinetics for a multilayered scale was proposed. The model predictions showed good agreement of calculated and experimental oxidation kinetic curves. It was shown that increase of oxidation resistance of triple ceramics (ZrB_2–SiC–$ZrSi_2$) is due to decreased oxygen diffusion rate in subsurface layer. The role of the subsurface layer is enhanced by the fact that this layer is more uniform in thickness compared with the outer layer of glass which is varied in thickness up to discontinuity. Comparison with experimental data shows that calculated model parameters fully correspond to physical meaning of the oxidation process.

Acknowledgement

This work was carried out under Science and Technology Centre of Ukraine Project P286.

References

1. Lavrenko VA, Panasyuk AD, Protsenko TG, et al. High-temperature reactions of materials of ZrB_2–$ZrSi_2$ system with oxygen. *J Powder Metall Met Ceram* 1982;**21**(6):471–3.
2. Lavrenko VA, Dayatel VD, Lugovskaya ES. Interaction of materials ZrB_2–$ZrSi_2$ system with oxygen at high temperature. *Powder Metall* 1982;**6**:56–8 [transl. from Russian].
3. Talmy IG, Zaykovski JA, Opeka MM. High-temperature chemistry and oxidation of ZrB_2 ceramics containing SiC, Si_3N_4, Ta_5Si_3, and $TaSi_2$. *J Am Ceram Soc* 2008;**91**(7):2250–7.

4. Peng F, Speyer RF. Oxidation resistance of fully dense ZrB_2 with SiC, TaB_2, and $TaSi_2$ additives. *J Am Ceram Soc* 2008;**91**(5):1489–94.
5. Talmy IG, Zaykovski JA, Opeka MM, Smith AH. Properties of ceramics in the system ZrB_2–Ta_5Si_3. *J Mater Res* 2006;**21**(10):2593–9.
6. Guo SQ, Nishimura T, Mizuguchi T, Kagawa Y. Mechanical properties of hot pressed ZrB_2–$MoSi_2$–SiC composites. *J Eur Ceram Soc* 2008;**28**(9):1891–8.
7. Guo SQ, Kagawa Y, Nishimura T, Tanaka Y. Pressureless sintering and physical properties of ZrB_2-based composites with $ZrSi_2$. *J Eur Ceram Soc* 2009;**29**(4):787–94.
8. Opila E, Levine S, Lorincz J. Oxidation of ZrB_2- and HfB_2-based ultra-high temperature ceramics: effect of Ta additions. *J Mater Sci* 2004;**39**:5969–77.
9. Talmy IG, Zaykovski JA, Opeka MM, Dallek S. Oxidation of ZrB_2 ceramics modified with SiC and Group Iv-Vi transition metal borides. In: McNallan M, Opila E, editors. *High temperature corrosion and material chemistry III*. Pennington, NJ: The Electrochemical Society, Inc.; 2001. p. 144.
10. Guo S-Q, Kavagava Y, Nishimura T. Mechanical behaviour of two-step hot-pressed ZrB_2-based composites with $ZrSi_2$. *J Eur Ceram Soc* 2009;**29**:787–94.
11. Grigoriev ON, Gogotsi Yu, Brodnikovsky G, Subbotin VI NP. Development and properties of SiC-B4C-MeB2 ceramics. *Powder Metall* 2000;**5/6**:29–42 [transl. from Russian].
12. Reshetnyak MV, Sobol OV. Expansion of possibilities for analysis of structure and substructural characteristics of nanocrystalline condensed and massive materials of quasibinary W_2B_5-TiB_2 system using XRD data processing code "New_Profile". *Phys Eng Surf* 2008;**3–4**:180–8 [in Russian].
13. Okamoto H, Si–Zr system. ACerS-NIST Phase Equilibria Diagrams, NIST Standard Reference Database 31.
14. Chamberlain AL, Fahrenholtz WG, Hilmas GE, Ellerby D. Oxidation of ZrB_2–SiC ceramics under atmospheric and reentry conditions. *Refract Appl Trans* 2005;**1**(2):2–8.
15. Dybkov VI. *Reaction diffusion and solid state chemical kinetics*. Kiev: IPMS Publ.; 2002, 127 p.
16. Galanov BA, Ivanov SM, Kartuzov EV, Kartuzov VV, Nickel KG, Gogotsi YG. Model of oxide scale growth on Si_3N_4 ceramics: nitrogen diffusion through oxide scale and pore formation. *Comput Mater Sci* 2001;**21**(1):79–85.